Geological data from the Western Afar Margin, East Africa (https://doi.org/10.5880/fidgeo.2020.017)

Frank Zwaan[1], Giacomo Corti[2], Federico Sani[1], Derek Keir[3], Ameha Atnafu Muluneh[4], Finnigan Illsley-Kemp[5], Mauro Papini[1]

1. *University of Florence, Italy*
2. *CNR Italian Research Council, Florence, Italy*
3. *University of Southampton, Southhampton, United Kingdom*
4. *Addis Ababa University, Ethiopia*
5. *Victoria University, Wellington, NZ*

1. Licence

2. Citation

When using the data please cite it as following:

Zwaan, F., Corti, G., Sani, F., Keir, D., Muluneh, A. A., Illsley-Kemp, F., & Papini, M. (2020): (2020): Geological data from the Western Afar Margin, East Africa. GFZ Data Services. https://doi.org/10.5880/fidgeo.2020.017

The data are supplementary material to:

Zwaan, F., Corti, G., Sani, F., Keir, D., Muluneh, A. A., Illsley-Kemp, F., & Papini, M. (2020). Structural Analysis of the Western Afar Margin, East Africa: Evidence for Multiphase Rotational Rifting. Tectonics, 39(7). https://doi.org/10.1029/2019TC006043

Table of contents

3. Data Description

This dataset contains geological data from the Western Afar Margin (WAM) in East Africa. These include (reprocessed) earthquake data from previously published surveys and publically accessible databases (Keir et al. 2006, 2009; Ebinger et al 2008; Belachew et al. 2011; Illsley-Kemp et al. 2018a, b and the GCMT Project 2019), which form the basis for Seismic Moment Release (SMR) mapping as well as and tectonic stress analysis, revealing the location and intensity of ongoing deformation, as well as the direction of current extension, respectively. In addition, we present various large-scale maps of the WAM, depicting faults, dikes and sedimentary basins as interpreted from topographic indicators

Field data (GPS locations, fault measurements, field book), acquired during two field campaigns in Ethiopia and Eritrea are included, as well as the kinematic interpretation of the field data using Wintensor software (Delvaux & Sperner 2003). These results are combined with previously published kinematic data from Eritrea and Ethiopia (i.e. the northernmost and southern segments of the WAM, studied by Chorowicz et al. 1999 and Sani et al. 2017), yielding the first coherent overview of (current) tectonic deformation covering the whole margin. Note that we also provide a field book with detailed descriptions of every outcrop, including photographs. Finally, we include unique borehole data from the Kobo graben area, based on well logs from irrigation projects kindly provided to us by local geologists during the Ethiopian field campaign (see section 2.5 and the acknowledgements) . Applications and interpretation of the data provided in this dataset can be found in Zwaan et al. (2020).

3.1. Earthquake analysis

Data from earthquake surveys (Belachew et al. 2011 and Illsley-Kemp et al. 2018a) were used to determine on-going deformation and active faults along the WAM. The seismicity data were relocated using the same method and velocity model as Illsley-Kemp et al. (2018a) method and are included in this dataset (**EarthquakeCatalogue_0713.txt**). This earthquake data is used for detailed analysis and cross-sections. Seismicity distribution maps (of both the whole dataset, as well as of a selection of earthquakes xyz error margins of <5 km in both directions, used for detailed analysis) are also included in this data publication. The earthquake catalogue is then expanded to include data from previous surveys (Keir et al., 2006) and this is used for seismic moment release (SMR) mapping, the results of which are provided in this dataset as well (EarthquakeCatalogue_0113.txt).

Focal mechanisms were used for calculating tectonic stress orientations. We provide maps of focal mechanism locations (focal mechanisms gathered from Keir et al. 2006; Illsley-Kemp et al., 2018a, b and the GCMT Project 2019), as well as maps and details on tectonic stress analysis (Fig. 1).
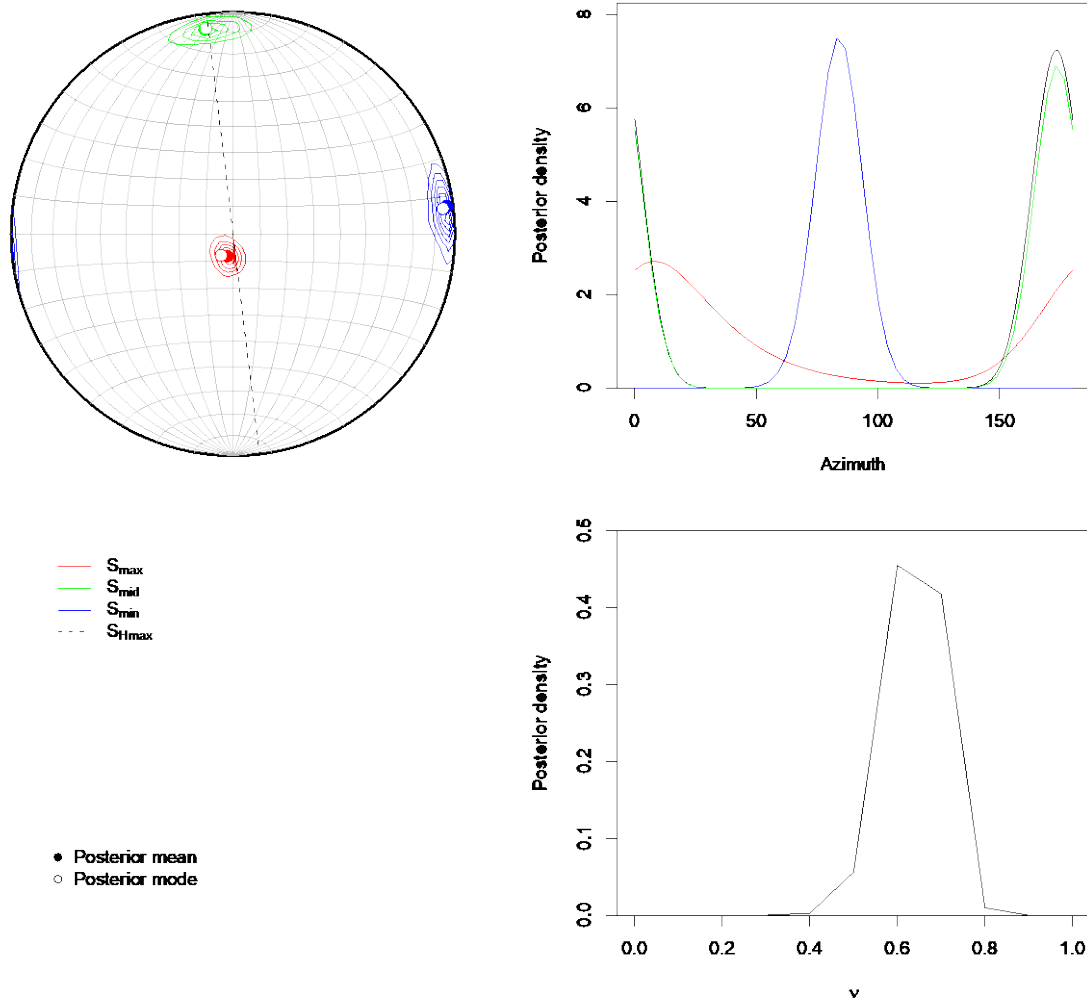
Fig. 1. Example of tectonic stress analysis of the WAM area based on earthquake focal mechanisms. Top left: Stereonet showing the geometric distribution of principal stress axes, lower-hemisphere projection, North is up, West is left. Red, green and blue contours denote S1, S2, and S3 respectively. The Black dashed line denotes the orientation of maximum horizontal stress (SHmax). Top right: Posterior distributions of the azimuths of the principal stress directions and SHmax. Bottom right: Posterior distribution for the stress ratio.

3.1.1. Earthquake file descriptions

EarthquakeCatalogue_0113.txt:

Column name	Unit/notation	Description
Date	yyyymmdd	Date of seismic event
Time	hh:mm:ss	Time of seismic event
Latitude	DD.xxxx	Latitude (WGS 84) of earthquake epicenter
Longitude	DD.xxxx	Longitude (WGS84) of earthquake epicenter
Depth	Km	Earthquake hypocentre depth
Magnitude		Earthquake magnitude
SeismicMoment(10**)	Nm	Seismic moment release (SMR)

EarthquakeCatalogue_0713.txt:

Column name	Unit/notation	Description
Date	yyyymmdd	Date of seismic event
Time	hh:mm:ss	Time of seismic event
Latitude	DD.xxxx	Latitude (WGS 84) of earthquake epicenter
LatErr	km	Latitude error of earthquake epicenter
Longitude	DD.xxxx	Longitude (WGS84) of earthquake epicenter
LongErr	km	Longitude error of earthquake epicenter
Depth	km	Earthquake hypocenter depth
DepthErr	km	Depth error of hypocenter
Magnitude	Local Magnitude	Earthquake Magnitude

AfarRift_2011-2013_FocalMechanisms.txt (Illsley-Kemp et al. 2018b),
AfarRift_GlobalCatalogue_FocalMechanisms.txt (GCMT Project 2019),
MainEthiopianRift_FocalMechanisms.txt (Keir et al. 2006),
WesternAfarMargin_AFAR20112013_FocalMechanisms.txt (Illsley-Kemp et al. 2018a): WesternAfar-
Margin_GlobalCatalogue_FocalMechanisms.txt (GCMT Project 2019),

Column name	Unit/notation	Description
ID	-	Seismic event ID
Date	dd/mm/yyyy	Date of seismic event
Time	hh:mm:ss	Time of seismic event
Latitude	DD.xxxx	Latitude (WGS 84) of earthquake epicentre
LatErr*	*km*	*Latitude error**
Longitude	DD.xxxx	Longitude (WGS84) of earthquake epicentre
LongErr*	*km*	*Longitude error**
Depth	km	Earthquake hypocentre depth
DepthErr*	km	Depth error*
Magnitude		Earthquake magnitude
Strike	Degrees	Strike of the nodal plane
Dip	Degrees	Dip of the nodal plane
Rake	Degrees	Rake of the nodal plane
T_plunge	Degrees	Plunge of the T-axis
T_azimuth	Degrees	Azimuth of the T-axis
P_plunge	Degrees	Plunge of the P-axis
P_azimuth	Degrees	Azimuth of the P-axis
B_plunge	Degrees	Plunge of the B-axis
B_azimuth	Degrees	Azimuth of the B-axis

* Not provided in every file

3.2. Mapping

Large-scale geological mapping (sedimentary basins, faults, dikes and potential sedimentary contacts) was performed on the basis of SRTM and ASTER topography data (available via https://earthexplorer.usgs.gov) in QGIS (www.qgis.org), with the help of Google Earth Pro satellite imagery and previously published data (see details in Zwaan et al. 2020). Various major and minor sedimentary basins occur along the WAM, defined as areas with an inclination of < 5˚. We provide a map with the locations and names of the major sedimentary basins, (i.e. the marginal grabens and main sub-basins) as well as a table with details such as basin size, altitude and orientation. NB: the extent of sedimentary the marginal graben structures does not always coincide with the extent of the marginal graben structures. We also provide a more detailed digital map with all sedimentary basins along the margin (according to the < 5˚ inclination definition). We provide both PDF and digital maps concerning these various features along the WAM.

3.3. Fieldwork data

Fieldwork data (measurements on faults along the WAM) from two field campaigns (one in Eritrea, and one in Ethiopia) are presented in table form (see column description of **Fault_field_data.xls** and Fig. 2 below). Next to that, we provide an overview of the numerous stops from the 2018 Ethiopian campaign (see **Field_stops.pdf** description below), as well as a detailed field book (**Field_book.pdf**), which provides a systematic record of all relevant geological observations and interpretations, including photographs of every visited outcrop. We also provide a detailed roadmap based on satellite imagery (with secondary and tertiary roads, so far not digitized in e.g. Google Maps) that was used for navigation in the field, as well as GPS locations of every stop (see **Field_stops.pdf** description below for the various definitions).

3.3.1. Field Work files description

Fault_field_data.xls:

Column name	Unit/notation	description
stop (FZ)		Field stop according to "Field_stops.docx" available in the same folder
lat	DD.xxxx	Latitude (WGS 84)
lon	DD.xxxx	Longitude (WGS84)
Type	-	D = Dike, I = inverse fault, N = normal fault
Azimuth	degree	Azimuth of fault plane
Dip	degree	Dip of fault plane
Pitch	degree	Pitch of striae measured on fault plane (see Fig. 2)
Rake	degree	Rake of striae measured on fault plane (see Fig. 2)

Field stops.pdf:

This file provides a complete overview of stops of the Ethiopia 2018 Fieldwork. Note that we use different notations for the various stops and points (Fig. 3). The table is based on the GPS points as recorded by Federico Sani (GPS FS), from which the coordinates are adopted (latitude and longitude, both in decimal degrees, WGS 84 convention), see (**GPS_points_FS_kmz**). Giacomo Corti (GC) used a tablet with GPS function and digital maps that served for both navigation and field notes. These points (starting with "ET-2018-" followed by a number) are given in a separate column, and provided as a kmz file

together with the fieldwork trail (GPS_points_GC). Several of the GPS FS points do not only refer to geological sites, whereas the GPS-GC points lack various data points. Therefore, the field day-based coding (1.1, 1.2, 2.1, …) used by Frank Zwaan was adopted for the Zwaan et al. (2020) publication.
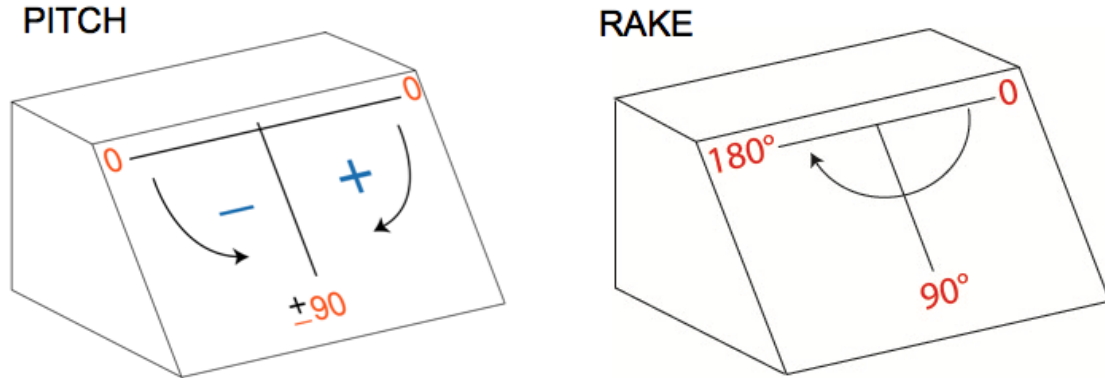
Fig. 2. Definition of pitch (left) and rake (right). Both describe the relationship between the strike of a given fault plane and the directions of kinematic indicators on the same fault plane. Pitch is defined between 0 and +/- 90˚, with a letter I, N, D, or S indicating the type of motion (Inverse, Normal, Dextral of Sinistral). Rake is defined as an angle between 0 and 180˚ and is positive for an inverse fault, while negative for a normal fault. Pitch values were measured in the field and subsequently converted to Rake values for Wintensor analysis. Example: a -70˚ N pitch value translates to a -110˚ Rake value.

3.4. Fault data analysis

The fieldwork data were analysed with Wintensor (Delvaux & Sperner 2003, last version and background info available at: http://damiendelvaux.be/Tensor/WinTensor/win-tensor.html) to determine the associated stress regime. We provide a zip-folder containing the original ".wtd" files for every outcrop, that can be opened in Wintensor, as well as a text editor. Name convention: WAM_(field stop).wtd. NB: in some cases, the data are split in two (e.g. a normal vs. inverse fault, or a NE vs NW orientation). We provide the results of our stress analysis in table form (**WAM_extension_overview_table.pdf**). These are combined with data from Chorowicz et al. (1999) and Sani et al. (2017), which are also included in the table, into an overview of recent extension along the WAM. NB: Chorowicz et al. (1999) also proposes earlier phases of extension with different orientations (see Zwaan et al. 2019) for details). We also provide GPS locations associated with the fault data from Chorowicz et al. (1999) and Sani et al. (2017). NB: the Chorowicz et al. (1999) locations are estimations from the maps presented in their publication.

3.5. Well data

During the Ethiopian field campaign, unique well data were acquired with help from Said Abdu (Water Resource Mine and Energy office of Tigray, Alamata), Fanuel Sharew, Abrha Shumey and Berhe Abrha (Water Resource Mine and Energy office of Raya Azebo, Mahoni) and Solomon Arbsie (Kobo Girana Valley Development Program, Kobo). A map shows the locations of the wells, and an overview of the

well data itself (exact locations, well depth, altitude, depth of bedrock) is presented in table form. We also provide .kmz files with the locations of all wells.

4. File structure

This data publication consists of 92 files: (digital) maps, GPS locations, tables, text and Wintensor files. A detailed overview of all files within this dataset is given in the **List of Files.**

5. Acknowledgements and funding

6. References

Belachew, M., Ebinger, C., Coté, D., Keir, D., Rowland, J.V., Hammond, J.O.S., Ayele, A. 2011. Comparison of dike intrusions in an incipient seafloor-spreading segment in Afar, Ethiopia: Seismicity perspectives. Journal of Geophysical Research: Solid Earth 116, B06405. https://doi.org/10.1029/2010JB007908

Chorowicz, J., Collet, B., Bonavia, F., Korme, T., 1999. Left-lateral strike-slip tectonics and gravity induced individualisation of wide continental blocks in the western Afar margin. Eclogae Geologicae Helvetiae, 92, 149-158. https://doi.org/10.5169/seals-168656

Delvaux, D., Sperner, B. 2003. Stress tensor inversion from fault kinematic indicators and focal mechanism data: the TENSOR program. In: Nieuwland, D. (ed) New Insights into Structural Interpretation and Modelling. Geological Society, London, Special Publications, 212, 75-100. https://doi.org/10.1144/GSL.SP.2003.212.01.06

Ebinger, C.J., Keir, D., Ayele, A., Calais, E., Wrigth, T.J., Belachew, M., Belachew, M., Hammond, J.O.S., Campbell, E., Buck, W.R. 2008. Capturing magma intrusion and faulting processes during continental rupture: seismicity of the Dabbahu (Afar) rift. Geophysical Journal International, 174, 1138-1152. https://doi.org/10.1111/j.1365-246X.2008.03877.x

GCMT (Global Centroid-Moment-Tensor [CMT]) Project, 2019. Website: https://www.globalcmt.org/

Illsley-Kemp, F., Keir, D., Bull, J.M., Gernon, T.M., Ebinger, C., Ayele, A., Hammond, J.O.S., Kendall, J.-M., Goitom, B., Belachew, M. 2018a. Seismicity during continental breakup in the Red Sea rift of Northern Afar. Journal of Geophysical Research: Solid Earth, 123, 2345– 2362. https://doi.org/10.1002/2017JB014902

Illsley-Kemp, F., Bull, J.M., Keir, D., Gerya, T., Pagli, C., Gernon, T., Ayele, A., Goitom, B., Hammond, J.O.S., Kendall, J.M. 2018b. Initiation of a Proto-transform Fault Prior to Seafloor Spreading. Geochemistry, Geophysics, Geosystems 19, 4744–4756. https://doi.org/10.1029/2018GC007947

Keir, D., Ebinger, C.J., Stuart, G.W., Daly, E., Ayele, A. 2006. Strain accommodation by magmatism and faulting as rifting proceeds to breakup: Seismicity of the northern Ethiopian rift. Journal of Geophysical Research 111, B05314. https://doi.org/10.1029/2005JB003748

Keir, D., Hamling, I.J., Ayele, A., Calais, E., Ebinger, C., Wright, T.J., Jacques, E., Mohamed, K., Hammond, J.O.S., Belachew, M., Baker, E., Rowland, J.V., Lewi, E., Bennati, L. 2009. Evidence for focused magmatic accretion at segment centers from lateral dike injections captured beneath the Red Sea rift in Afar. Geology 37, 59-62. https://doi.org/10.1130/G25147A.1

Sani, F., Ghinassi, M., Papini, M., Oms, O., Finotello, A. 2017. Evolution of the northern tip of Afar triangle: inferences from the Quaternary succession of the Dandiero – Massawa area (Eritrea). Tectonophysics 717, 339-357. https://doi.org/10.1016/j.tecto.2017.08.026

Zwaan, F., Corti, G., Sani, F., Keir, D., Muluneh, A. A., Illsley-Kemp, F., & Papini, M. (2020). Structural Analysis of the Western Afar Margin, East Africa: Evidence for Multiphase Rotational Rifting. Tectonics, 39(7). https://doi.org/10.1029/2019TC006043